A simple evaluation of adiabatic proton tunneling across the electrified double layer

Mahsa Askari,[†,‡] Reagan C. Huckabee,[†,‡] and Joseph A. Gauthier[*,†]

†*Department of Chemical Engineering, Texas Tech University, Lubbock, TX 79409, USA*

‡*Contributed equally to this work*

E-mail: joe.gauthier@ttu.edu

Abstract

Coupled proton-electron transfer (CPET) reactions are likely to play a pivotal role in the global transition to a sustainable energy future. Our atomic scale understanding of this class of reactions has been significantly improved by developments in density functional theory (DFT) simulations. The ultimate goal of such simulations is to intelligently predict rates of CPET reactions at the electrified double layer, leading to the design of new catalysts. These studies often utilize harmonic transition state theory (HTST), which assumes that quantum tunneling through energy barriers is negligible. In this study, we present a simple evaluation of the contribution of quantum tunneling in the adiabatic limit of CPET reactions. We investigate the effect of different potential profiles on tunneling probabilities and compare these profiles with calculated CPET minimum energy paths (MEPs). We find that the calculated CPET MEPs can be significantly stiffer than the commonly used Eckart profile, and study the effect of changing barrier height and width on overall zero curvature tunneling correction factors. Depending on the reaction of interest and the bulk pH, proton tunneling can be a non-negligible phenomenon for CPET reactions at the electrified double layer. In particular, reactions involving large barriers are predicted to have significant contributions from non-classical tunneling, possibly explaining observed kinetic isotope effects for the hydrogen evolution reaction (HER) in alkaline media. Our model choices are significantly simplified – for example, neglecting the effects of reaction coordinate curvature and vibronic coupling – suggesting that our predicted tunneling contributions may be underestimated. However, our findings provide a simple way to evaluate whether tunneling is relevant for a particular CPET reaction of interest.

Introduction

Coupled Proton-Electron Transfer (CPET) reactions are a fundamental process where a proton and an electron are transferred simultaneously in a single kinetic step.[1–3] Such reactions can facilitate more sustainable routes for chemical transformations,[4–7] potentially reducing

the carbon footprint associated with processes critical to climate change mitigation efforts. Identifying and reducing rate-limiting steps for processes involving CPET steps remains a key challenge towards improving existing chemical transformation technologies.[3,8–11] Recent advancements in electrocatalysis theory and developments in methods for density functional theory (DFT) have revolutionized our understanding of CPET reactions at the atomic level.[3,11–24] These developments have not only provided fundamental insights into reaction dynamics but also improved our ability to predict trends in their rates more accurately, a crucial step towards optimizing the use of such processes in energy conversion and storage. Ultimately the goal of such approaches is to identify pathways to improve the efficiency of electrocatalytic processes, thereby improving their economic competitiveness and enabling their broader integration in the global transition to a sustainable energy system.[25–34]

The effective design of electrocatalysts, which accelerate the rate of processes involving CPET reactions, depends on predicting reaction rates. Fundamental rate equations are determined in part by activation barriers, in addition to overall reaction energies and their dependence on the applied potential. In particular, rates are defined by Gibbs free energies, requiring estimation of entropy at each point along the reaction coordinate. The entropy's influence on activation barriers, especially considering solvation effects and the accuracy of harmonic approximations, continues to be a dynamic field of study.[35–37] In practice, current research largely utilizes the relatively straightforward harmonic transition state theory (HTST) for analysis, which invokes several key assumptions:[38]

- Born-Oppenheimer (BO) approximation (i.e., non-adiabatic effects[39] are negligible)
- The reactant space is Boltzmann distributed (i.e., it is thermally equilibrated)
- Once the system crosses the reaction plane, there are no re-crossing events
- Quantum tunneling is negligible

There are limiting instances where the BO approximation fails to apply, particularly in molecular reactions involving hydrogen or proton transfer.[40–42] However, accurately de-

termining key parameters, especially in calculating solvation entropy, presents substantial difficulties in the absence of BO approximation. Here, we restrict our analysis to the case of adiabatic[43,44] tunneling, i.e. presuming the validity of the BO approximation, and furthermore invoking the aforementioned assumptions related to the reactant space thermal equilibration and no-recrossing of the reaction plane. We note that we are not necessarily suggesting that the BO approximation is valid for CPETs. Rather, we acknowledge that the BO approximation is commonly invoked in studying these reactions, and seek to evaluate the significance of proton tunneling within this simplified adiabatic limit.

Investigations into tunneling rates for reactions including N_2 dissociation on Ru[45] found that for heavier atoms like N, the impact of tunneling is negligible.[46] In part, this is because tunneling rates decrease exponentially with the particle mass. However, this principle suggests, potentially, a different scenario for proton transfer reactions, given its lower mass. For these lighter particles, tunneling could play a more significant role.[47,48] Very early studies related to hydrogen or proton tunneling across the electrified double layer made strong assumptions regarding the characteristics of the activation barrier, such as its width, height, and shape.[49–53] These early theoretical models relied on specific potential profiles, like the Eckart[54] and harmonic (i.e., parabolic)[55–59] potentials, to describe the tunneling process, with predicted contributions from tunneling varying considerably. More recent studies[60,61] have revisited the influence of tunneling effects in reactions involving the transfer of hydrogen atoms or protons, suggesting that potentially revising the assumptions made by HTST could be beneficial.

For CPET reactions in particular, experimental investigations employing isotope-labeled techniques (e.g., comparing reaction rates in H_2O versus D_2O) yield varied results and typically concentrate on a single reaction, for instance, the hydrogen evolution reaction (HER).[49] In experimental studies of even relatively simple reactions like the HER, researchers face significant challenges, beyond the expense of isotopically pure deuterated water. A major issue is that the measured current densities do not solely reflect the kinetics of an elementary re-

action step,[62,63] particularly at high overpotential where bubble formation on the electrode surface can drastically reduce the availability of active sites for the reaction to occur. This complexity underscores the difficulty in isolating and analyzing the contributions of individual steps within the reaction mechanism, highlighting the value in theoretical studies to really probe a single reaction.[64]

In this study, we conduct a comparative analysis of different potential profiles – specifically, Eckart, Heaviside, linear, and harmonic (parabolic) – to examine their behavior relative to calculated minimum energy paths (MEPs) of CPET reactions across the electrified double layer. Our goal is to assess the influence of potential energy surface (PES) configurations on tunneling probabilities. We compute zero curvature tunneling[65,66] correction factors $\Gamma(T)$ for each potential profile, with a focus on understanding the role of barrier height and tunneling distances in modulating these factors, particularly close to ranges relevant for CPET reactions. Using the general trends with barrier height, width, and profile, we model CPET reduction reactions on several noble metals to estimate the extent of tunneling under reaction conditions. Our calculations utilize both alkaline and acidic environments, and focus on pathways relevant to sustainability and decarbonization. Our results suggest that, for certain reactions, tunneling rates may contribute significantly to the overall reaction rate, particularly in scenarios of low overpotential. Our model of tunneling is quite simple in comparison to state-of-the-art theoretical methods typically utilized for molecular systems which include non-adiabatic effects such as reaction coordinate curvature, vibronic coupling. As such, our model may underestimate actual tunneling rates. Nevertheless, we explore how our theoretical insights align with experimental observations, especially concerning kinetic isotope effects, and discuss the potential for tunneling to remain undetected, contingent on the rate-determining steps of the reactions under study.

Methods

Density functional theory details

All DFT calculations were executed utilizing the Vienna Ab initio Simulation Package (VASP),[2,67–69] integrated with the Atomic Simulation Environment (ASE).[70] In our simulations, the core electrons of each atom were represented as Projector Augmented Wave (PAW) pseudopotentials.[71,72] Valence electrons were expanded as planewaves up to a kinetic energy cutoff of 500 eV. Electron exchange and correlation interactions were taken into account by employing the revised Perdew-Burke-Ernzerhof (RPBE) exchange-correlation functional of Hammer and Nørskov.[73] For bulk lattice constant optimizations, the Brillouin zone was sampled using a $(12 \times 12 \times 12)$ Monkhorst-Pack[74] Γ centered k-point mesh. Cell vectors were optimized until the total energy changed by less than 10^{-7} eV between iterations. CPET reactions were probed in a $(3 \times 4 \times 3)$ supercell, with the Brillouin zone sampled with a $(4 \times 3 \times 1)$ Monkhorst-Pack Γ centered k-point mesh. All metals considered were face centered cubic – Ag, Au, Cu, and Pt. All DFT calculation input and output files can be found in an electronic Supporting Information (SI) archive with this article, separate from the written SI.

Geometry optimizations for energetic minima (e.g., initial and final states) were considered to be converged when the forces on each unconstrained atom were less than 0.03 eV/Å. The adsorption Gibbs free energies ΔG for reaction intermediates are computed through this specific formula:

$$\Delta G = \Delta E + \Delta \mathrm{ZPE} - T\Delta S \tag{1}$$

Here, ΔE represents the electronic energy difference for the species once adsorbed, ΔZPE denotes the change in zero-point energy, and ΔS refers to the entropy change of the adsorbed entities relative to the surface of the catalyst. The calculation of zero-point energies (ZPE) and entropies (S) was conducted under the harmonic oscillator approximation, with translational and rotational degrees of freedom neglected.

Constant potential calculations in the grand canonical ensemble

CPET reactions were probed using DFT in the grand canonical ensemble (GC-DFT). More detail on the theory behind these calculations can be found in our previously published work,[18–20,75] in addition to work from other groups.[11,16,76–78] Briefly, we treat solvation via a hybrid explicit-implicit model, i.e., 'micro-solvation,' wherein a small cluster of explicit water molecules contribute hydrogen bonding and solvation of ions (e.g., hydronium and hydroxide), with the remaining solvation contributions being captured by a polarizable continuum model as implemented in VASPsol.[16,76] We illustrated transition state geometries in chemical reactions with Figures S6 and S7, contrasting estimated MEPs via constant potential FBL against actual saddle points localized using the improved Dimer method by Henkelman[79] in SI Note 3. Utilizing optimization routines available in our public Github repository,[80] the number of electrons in the simulation is optimized to achieve a desired potential, and countercharge placed by solving the linearized Poisson-Boltzmann equation. With the potential set, the desired DFT optimization is then carried out – constrained or unconstrained geometry optimization (for localizing energetic minima), or saddle point search routines, e.g., the Dimer method.[81] The number of electrons is periodically adjusted such that the end result is a self-consistent constant potential energetic minima or saddle point routine. The energetic contribution of bringing in excess electrons from an external reservoir is calculated via the grand canonical free energy,

$$\Omega = E - q\Phi \quad , \tag{2}$$

where Ω is the grand canonical free energy, E the total energy from DFT, q the number of additional electrons from the external reservoir, and Φ the (absolute) potential of the external reservoir. The absolute potential is converted to a standard hydrogen electrode (SHE) reference by utilizing the absolute potential of the SHE, typically reported to be between 4.2 and 4.6 V.[82–85] Here, we choose a value of 4.43 V.

To determine CPET activation barriers using GC-DFT for each system investigated,

we first performed a series of fixed bond length calculations (1D-FBL), wherein the O–H bond length for the transferring proton is systematically stretched. For each point along the pathway, corresponding to a particular fixed O–H bond length, the geometry is optimized in the grand canonical ensemble subject to this constraint. This sequence of calculations serves several important purposes. First, the highest energy image along this path serves as an excellent estimate for the real transition state *energy*, in addition to the geometry, as we previously demonstrated[21] and shown in SI Note 3 for the systems studied here. The 1D-FBL is also significantly more accessible computationally when compared to a true saddle point search. Second, the estimated saddle point geometry from this routine, in addition to images before and after, provide an excellent initial guess for a dimer calculation, which localizes the true saddle point at constant potential. Third, given the above, the 1D-FBL band provides an estimate for the MEP and distance that the proton must move to cross the reaction coordinate. As we show in the Results and Discussion below, the tunneling correction factor is extremely sensitive to this distance, which is otherwise not a well-defined quantity. Finally, the 1D-FBL importantly can indicate whether a saddle point exists at all for the particular system/potential combination. To see this final point more clearly, consider the two 1D-FBL bands shown in Figure 1.

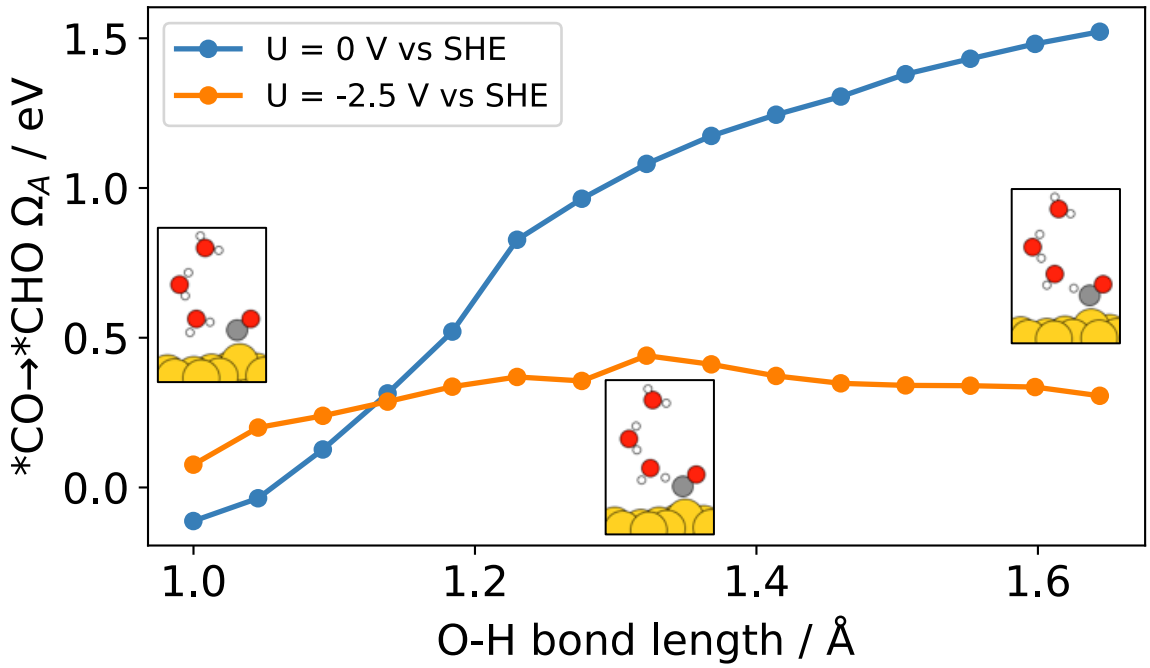

Figure 1: Examples of two constrained bond length (1D-FBL) calculations performed at constant potential, in this case for alkaline protonation of *CO to form *CHO on Au (111). In orange, performed at $U = -2.5$ V vs SHE, we see a clear local maximum corresponding approximately to a transition state. In contrast, the profile of the 1D-FBL performed at $U = 0$ V vs SHE shows no such local maximum, suggesting that there is no activation barrier at this potential.

In these two 1D-FBL bands, we illustrate two cases of alkaline *CO protonation to form *CHO, i.e.,

$$*\mathrm{CO} + \mathrm{H_2O} + e^- \rightarrow *\mathrm{CHO} + \mathrm{OH}^- \quad . \tag{3}$$

At an applied bias of $U = 0$ V vs SHE, we show a pathological example of a case where no barrier is found. Instead, the energy increases monotonically as the proton is transferred from the water molecule to the carbon atom. Here, it is crucial to note that the absence of a local minimum for the product state (i.e., the reverse reaction has zero barrier) suggests that the reaction will not proceed under these conditions. In such a case, no dimer calculation was performed, as it would be unlikely to localize a true saddle point. Contrasting this case, at an applied bias of $U = -2.5$ V vs SHE, we see a well-behaved 1D-FBL with a defined local

maximum along the band. This image provides an excellent guess of both the activation barrier (i.e., the energy of the true transition state) and the geometry. Combined with the image preceding the local maximum to generate a reaction coordinate vector, the dimer calculation beginning with this geometry converged to a saddle point in about 25 steps. All DFT calculation input and output files can be found in an electronic SI zip archive with this article, separate from the written SI.

Determination of adiabatic tunneling correction factors

Calculating zero curvature tunneling correction factors (Γ) first requires determination of the permeability function, $G(E)$, which approximately describes a tunneling probability for a particle at a particular energy E. The form of this permeability function is dependent on the barrier profile, its width, and its height. Further detail on the permeability function can be found in published literature.[86,87] Briefly, we treat the tunneling particle semiclassically and consider the adiabatic groundstate. Accounting for the possibility of nonclassical overbarrier reflection close to the barrier height E_0, we define an action integral $\theta(E)$,

$$\theta(E) = \frac{2\pi}{h} \int_{x_1}^{x_2} \sqrt{2m(V(x) - E)}\, dx \quad . \tag{4}$$

Here, h is the Planck constant, m the mass of the tunneling particle, $V(x)$ the potential profile as a function of reaction coordinate position, and x_1 and x_2 the classical turning points (i.e., points along the reaction coordinate at which $V(x) = E$). From this action integral θ, we can then define the permeability function $G(E)$,

$$G(E) = \begin{cases} E < 0 & 0 \\ 0 \leq E \leq E_0 & \left(1 + \exp\left[2\theta(E)\right]\right)^{-1} \\ E_0 < E \leq 2E_0 & 1 - G\left(2E_0 - E\right) \\ E > 2E_0 & 1 \end{cases} \tag{5}$$

Following calculation of the permeability function, the zero-curvature tunneling correction factor Γ is defined as the ratio of the non-classical and classical reaction rates,

$$\Gamma(T) = \frac{k_{\text{non-classical}}}{k_{\text{classical}}} = \frac{\int_0^\infty \exp\left[-\beta E\right] G(E) dE}{\frac{1}{\beta}\exp\left[-\beta E_0\right]} \quad , \tag{6}$$

with $\beta = (k_B T)^{-1}$, where k_B is the Boltzmann constant and T the temperature. The numerator of this expression corresponds to the non-classical (i.e., zero curvature tunneling) rate, comprised of a Boltzmann weighting of the permeability function integrated over all possible energy levels. Given the form of the permeability function $G(E)$ in Eq. 5, the integral can be solved analytically for $E \geq 2E_0$, i.e.

$$\int_{2E_0}^{\infty} \exp[-\beta E] dE = \frac{1}{\beta}\exp\left[-2\beta E_0\right] \quad . \tag{7}$$

We then arrive at a simplified expression for Γ,

$$\Gamma(T) = \beta \exp\left[\beta E_0\right] \left(\int_0^{2E_0} \exp[-\beta E] G(E) dE + \frac{1}{\beta}\exp[-2\beta E_0] \right) \tag{8}$$

Given the expression in Eq. 8, the only degree of freedom remaining is to define the form of the barrier profile, $V(x)$. We consider several possible profile forms, including a Heaviside function, parabolic, linear, and the well-studied Eckart profiles. For comprehensive mathematical formulations of the Heaviside, linear, harmonic, and Eckart potentials utilized in this study, including their respective parameters, please refer to the SI Note 1. A more detailed discussion of the basic appearance of these profiles along with a comparison to actual MEPs for CPET reactions can be found in the Results and Discussion below. In general, we find that the form of the MEP for the CPET reaction to be only roughly approximated by the four general potential profiles considered here, with the CPET MEP at times being considerably sharper, particularly near the barrier peak, than the other profiles.

The Eckart potential is a profile of the form

$$V(x) = E_0 \operatorname{sech}^2\left(\frac{\pi x}{d}\right) \quad , \tag{9}$$

where E_0 is the barrier height and d the barrier width. From this potential profile, the permeability function can be analytically determined by solving the Schrödinger equation, as noted in reference literature,[38]

$$G(E) = \frac{\cosh\left(4\pi\alpha - 1\right)}{\cosh\left(4\pi\alpha\right) + \cosh\left(2\pi\delta\right)} \quad , \tag{10}$$

where

$$\alpha = \frac{d}{h}\sqrt{2mE} \quad , \tag{11}$$

and

$$\delta = \frac{1}{2}\sqrt{32mE_0\left(\frac{d}{h}\right)^2 - 1} \quad . \tag{12}$$

Additionally, we performed a numerical integration of the action integral (Eq. 4), subsequently applying the results in Eq. (5) to calculate $G(E)$ for the Eckart potential. Our approach will later allow for a benchmark of our numerical integration, by comparing analytical and numerical determinations of $G(E)$. A similar analysis for the other archetypical potential profiles discussed below, including analytical expressions for the classical turning points as a function of the energy E, can be found in SI Note 1.

All variables relevant to this work are comprehensively described in Table 1.

Table 1: List of Variables and Their Descriptions

Variable	Description
E	Energy of the particle
$V(x)$	Potential profile as a function of reaction coordinate, x
x_1, x_2	Classical turning points where $V(x) = E$
$\theta(E)$	Action integral between turning points x_1 and x_2
$G(E)$	Permeability function, describes tunneling probability
$\Gamma(T)$	Zero-curvature tunneling correction factor
d	Barrier width in the potential profile
E_0	Barrier height in the potential profile
β	Inverse temperature factor ($\beta = 1/(k_B T)$)
T	Absolute temperature used in calculations of $\Gamma(T)$
α	Parameter in Eckart potential related to mass and energy
δ	Parameter in Eckart potential related to potential form
q	Charge of the particle involved in the reaction

Results and Discussion

Archetypical potential profiles and benchmarking

The basic appearance of the potential profiles considered in this work, along with a comparison to a MEP for two examples of a CPET reaction is shown in Figure 2.

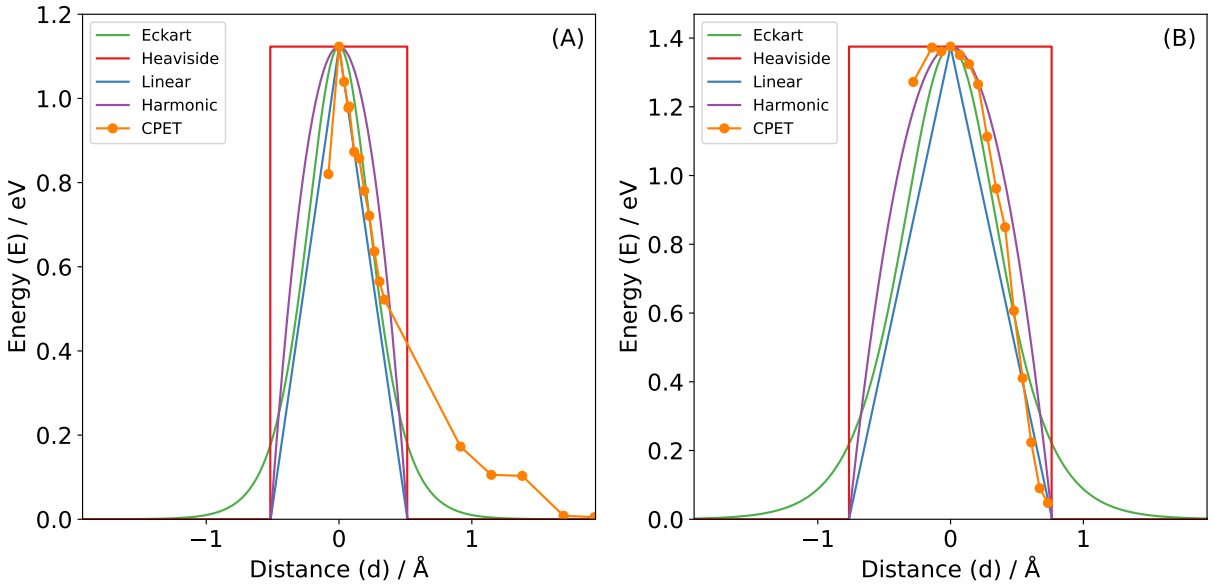

Figure 2: Comparison of possible forms for $V(x)$ with minimum energy paths for (A) $*\mathrm{CO} + \mathrm{H_2O} + e^- \rightarrow *\mathrm{CHO} + \mathrm{OH}^-$ on Cu (100) at $U = -1.413$ V vs SHE and (B) $* + \mathrm{H_2O} + e^- \rightarrow *H$ at $U = -2.0$ V vs SHE on Ag (111). These forms of $V(x)$ use a distance (d) that has been fit to the corresponding CPET MEP using least-squares regression.

The two CPET MEPs illustrated in Figure 2 (A) and (B) have quite different profiles. In particular, the CO protonation MEP shows an extremely sharp potential energy surface as the reaction coordinate approaches the transition state – even sharper than the 'linear' profile. In contrast, the Volmer[88] MEP on Ag (111) is significantly smoother, particularly near the saddle point, though we find that the archetypical potential profiles illustrated here qualitatively captures the behavior of the calculated CPET MEPs. Both profiles also highlight the stiff nature of these reaction coordinates, showing significantly shorter distances than were utilized in early works studying proton tunneling.

Given the above potential profile forms, we determined the permeability function $G(E)$ by first numerically integrating the action integral function $\theta(E)$ shown in Eq. 4, before passing $\theta(E)$ into the piecewise definition of $G(E)$ shown in Eq. 5. The resulting permability functions are illustrated below in Figure 3.

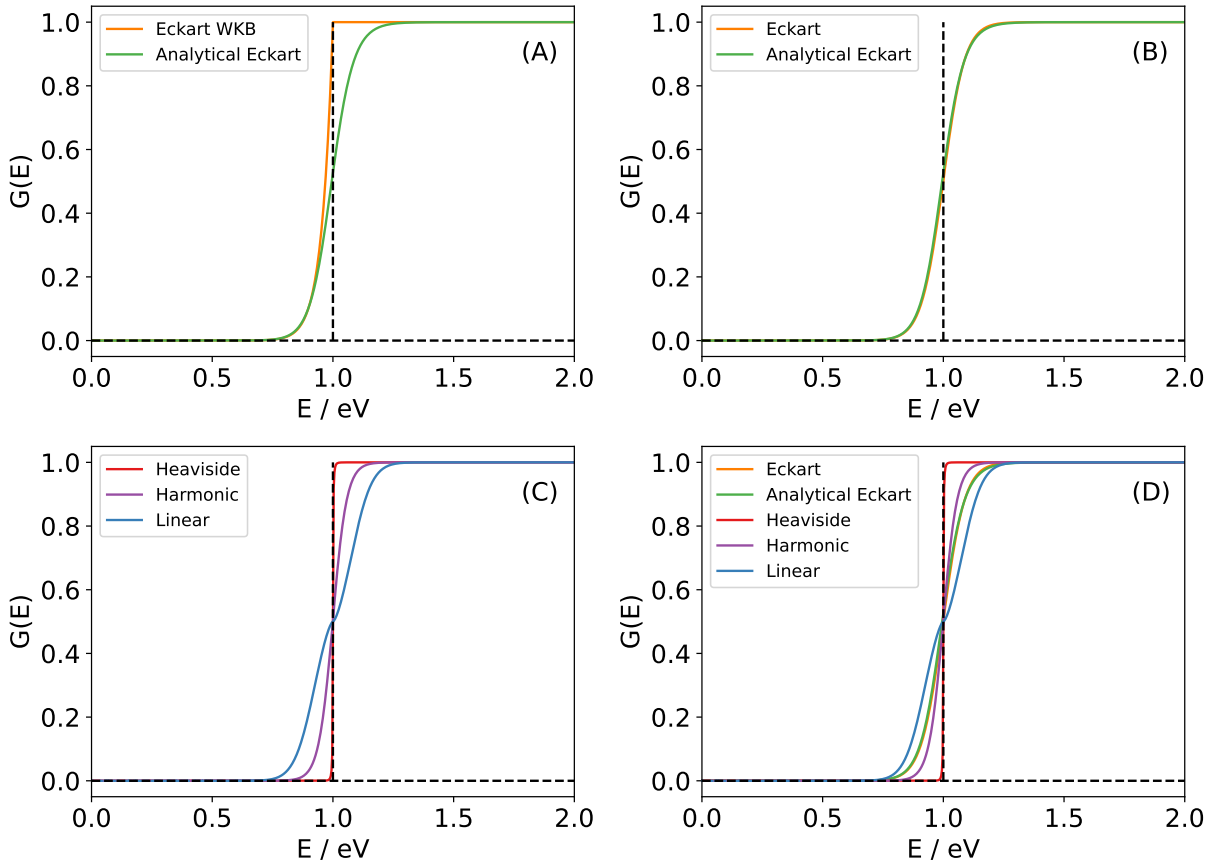

Figure 3: Computed permeability functions $G(E)$ for a barrier of height $E_0 = 1.6 \times 10^{-19} J$ and distance $d = 1.0$Å. A numerical determination of $G(E)$ using the WKB approximation is shown in (A), while the approach detailed in the methods section is shown in (B). Permeability functions for other potential profiles are shown in panels (C) and (D).

Figure 3 compares the solutions for permeability functions between varying potential profiles to see the impact of barrier shapes on the contribution of tunneling. $G(E)$ is plotted against energy levels and represents the solutions of the permeability function for Heaviside, Linear, Harmonic, and Eckart barriers. Commonly in very early literature reports on proton tunneling, the Wentzel-Kramers-Brillouin (WKB) approximation was used as a basis for estimating tunneling correction factors. Here, the major difference would be a different form

for $G(E)$ based on the action integral,

$$G(E) = \begin{cases} E \leq 0 & 0 \\ 0 \leq E \leq E_0 & \exp[-2\theta(E)] \\ E \geq E_0 & 1 \end{cases} . \tag{13}$$

A numerical solution to $G(E)$ for the Eckart potential profile when invoking the WKB approximation, compared to the previously discussed analytical solution, is shown in Figure 3(A). Here, we see excellent agreement for $E \ll E_0$, and a characteristic breakdown of the WKB approximation as $E \to E_0$. In contrast, the numerical solution shown in Figure 3(B), which uses the definition of $G(E)$ given in Eq. 5, shows excellent agreement with the analytical solution over all energy levels. Finally, panels (C) and (D) show the numerical solution for the other potential profiles considered here. In general, we find that the linear potential profile has the earliest onset of an increase in $G(E)$, in addition to having a higher probability of overbarrier reflection for $E > E_0$, while the Heaviside profile has a rapid but late onset of $G(E)$ and a relatively low probability of overbarrier reflection.

Defining a tunneling distance for CPET reactions

To compare the CPET MEP with the archetypical potential profiles in Figure 2, we defined a 'distance' metric; in this case, we choose the length of the O–H bond for the transferring proton. As we discuss in more detail below, this is a critical choice for the reaction coordinate, as the tunneling correction factor is extremely sensitive to the distance. Within our simplified framework, the appropriate distance to choose is the total displacement of all atoms between equilibrated initial and final states. In arriving at our chosen distance metric (i.e., the O–H bond length), we make several approximations and assumptions. First, we assume that the transferring proton is the only atom that moves across the reaction coordinate. In other words, the CPET involves only a proton transfer, without, for example, a concerted oxygen

or hydroxyl adsorption step. Atoms may reconfigure from initial to final states, but only the H atom moves significantly. Our second major assumption is related to the appropriate definition of the state containing an ion. For a charge transfer reaction, whether acidic or alkaline (i.e., whether hydronium is involved in the initial state, or whether hydroxide is produced in the final state, respectively), the true end state for the charged system is the ion in bulk solution, far from the interface. In contrast, in DFT calculations we model the charge transfer reaction by considering the ion in the reaction plane, or very close to it. There is an energetic cost associated with moving an ion from bulk solution to the interface, as has been reported in our prior work,[20,21,89] and as is illustrated below in Figure 4.

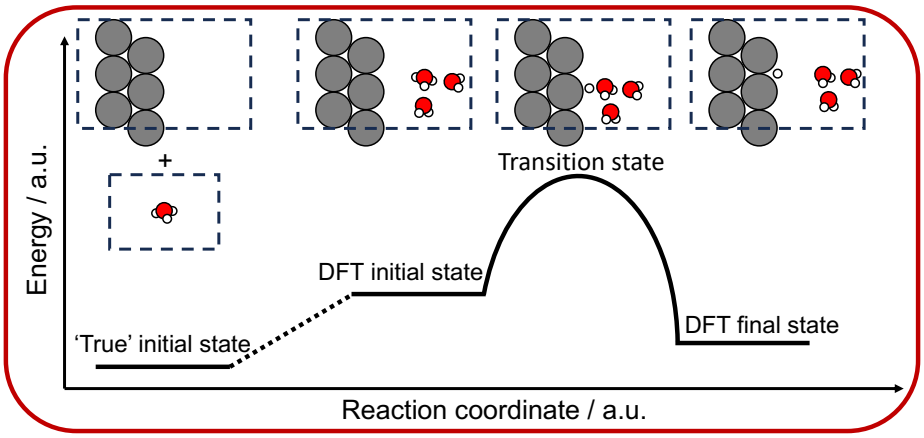

Figure 4: Illustration of a reaction coordinate for the acidic Volmer reaction, $(H^+ + e^-) + * \rightarrow H*$. The 'true' initial state is a proton in bulk solution far from the surface, and an electron in the metal, with a total charge $q = 1.0e$. In practice, this reaction step is modeled via the 'DFT initial state' with a hydronium molecule close to the reaction plane, typically with $q \approx 0.7e$.[89] There is a non-negligible energetic difference between the 'true' and 'DFT' initial states. A comparable concern is applicable in alkaline media, where the 'DFT' final state (hydroxide close to the interface) can be quite different in energy compared to the 'true' final state (hydroxide in bulk solution).[21,75]

Here, we illustrate the difference between the appropriate (quasi-)equilibrated initial state of the acidic Volmer reaction – i.e., $(H^+ + e^-) + * \rightarrow H*$, with the proton being in bulk solution far from the surface – and the initial state as modeled with DFT. For the latter, the hydronium is already in the reaction plane, and is partially hybridized with the surface, resulting in non-unity charge.[89] An analogous issue arises when considering alkaline

CPET reactions, in which water is the proton donor, and hydroxide is produced in the final state.[21,75] In such a case, the final state as modeled by DFT results in non-unity charge on the hydroxide and a non-negligible energy difference between the 'DFT' final state and 'true' final state. In our work, we essentially neglect the dashed portion of the reaction coordinate shown in Figure 4 from consideration in the distance metric. To validate this approximation, we determined the specific energy levels, relative to the barrier height, that contribute the most to the zero curvature tunneling correction factor Γ as defined in Eq. 8. In principle, all energy levels contribute to Γ; however, given the Boltzmann weighting factor in the integrand, at reasonable temperatures, very high energy levels are sparsely populated, and so may not contribute significantly to Γ. Similarly, low-lying energy levels are highly populated, but have a very low permeability function $G(E)$. As such, we calculated Γ by utilizing three separate energy bands, illustrated below in Figure 5.

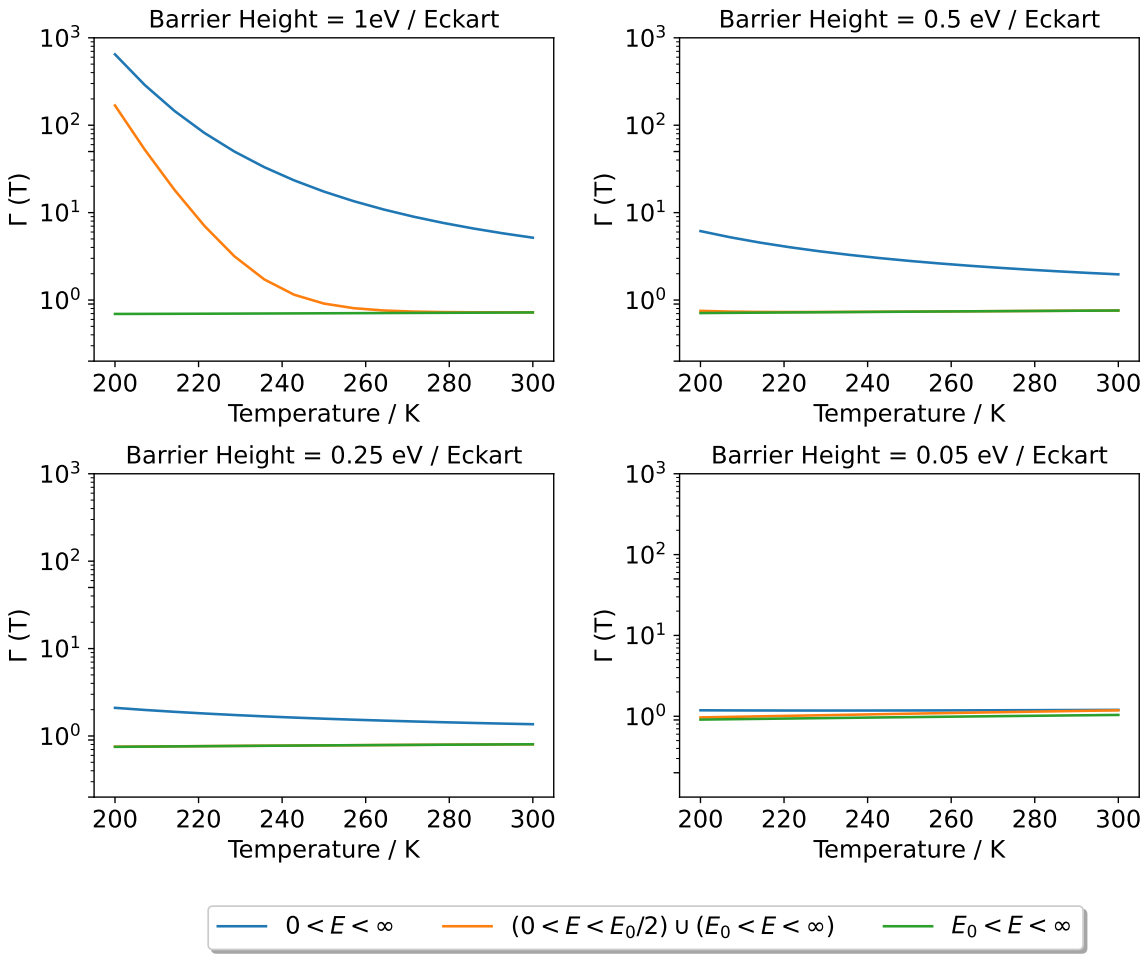

Figure 5: Contribution of different energy bands to the zero curvature tunneling correction factor Γ as a function of temperature and activation barrier height. Here, we assume an Eckart potential profile as detailed in the Methods section.

Here, the first energy band considered is all energies: $0 \leq E < \infty$ – i.e., the full zero curvature tunneling correction factor, shown in blue. We then consider Γ as calculated neglecting two energy bands. In orange, we show Γ as calculated by neglecting the integral over $\frac{1}{2}E_0 \leq E \leq E_0$, i.e., neglecting energy levels from half the barrier height to the full barrier height. Finally, in green we show Γ as calculated neglecting $0 \leq E \leq E_0$, i.e., all energy levels below the barrier height. We see that for high barriers ($E_0 > 0.5$ eV) Γ is dominated by states in the regime $\frac{1}{2}E_0 \leq E \leq E_0$, suggesting that the highly occupied, low-lying energy levels contribute negligibly to the overall tunneling correction factor. As such, we hypothesize that the energy difference between, e.g., hydronium in bulk solution vs hydronium in

the reaction plane, does not contribute substantially to the overall tunneling contribution to the reaction rate within our simplified scheme. This result supports our approximation of treating the 'distance' as it relates to tunneling with just the O–H bond length for the transferring proton, where the equilibrated initial state is approximated as either water or hydronium in the reaction plane, and the equilibrated final state is approximated as either hydroxide or water in the reaction plane. Following a similar line of logic, we also neglect the energetic penalty of adsorbate migration across the reaction coordinate. For example, ∗CO protonation to form ∗CHO on weak-binding fcc (111) surfaces involves ∗CO migrating from a hollow site to an atop site. However, we find the energetic penalty here to be very small, of the order k_BT, and so we do not consider such movement in our definition of the tunneling distance.

As an alternative to our approach, we could consider the characteristic distance as determined by Abild-Pedersen *et al.* in their recent work.[3] Here, they utilized *ab initio* molecular dynamics simulations to determine radial distribution functions of water-oxygen atoms relative to the z–coordinate of surface metal atoms as a function of surface hydrogen coverage. They determine characteristic distances of the order 3 to 4 Å, depending on the extent of hydrogen coverage. We note here that the actual tunneling distance should be shorter than this reported distance. For example, one should subtract, at the very least, the equilibrated initial state O–H bond length and radius of the metal surface atom, in which case the distance becomes comparable to the distances reported for CPET reactions here. Additionally, one may consider following the approach developed by Head-Gordon *et al.*,[90] where they report a quantifiable metric for determining when precisely a bond is broken, based on bond polarizability.

Evaluating the role of tunneling for CPET reactions across the electrical double layer

Following our analysis of the different potential profiles and their comparison to a calculated CPET MEP, we computed zero curvature tunneling correction factors $\Gamma(T)$ (see Eq. 8) for each profile. The resulting $\Gamma(T)$ surface for varying barrier height and tunneling distances is shown below in Figure 6. We note that the symbol d in Figures 6 - 9 represents the same barrier width discussed previously, and that all potential energy surfaces shown here are symmetric, i.e. the initial and final states are equilibrated.

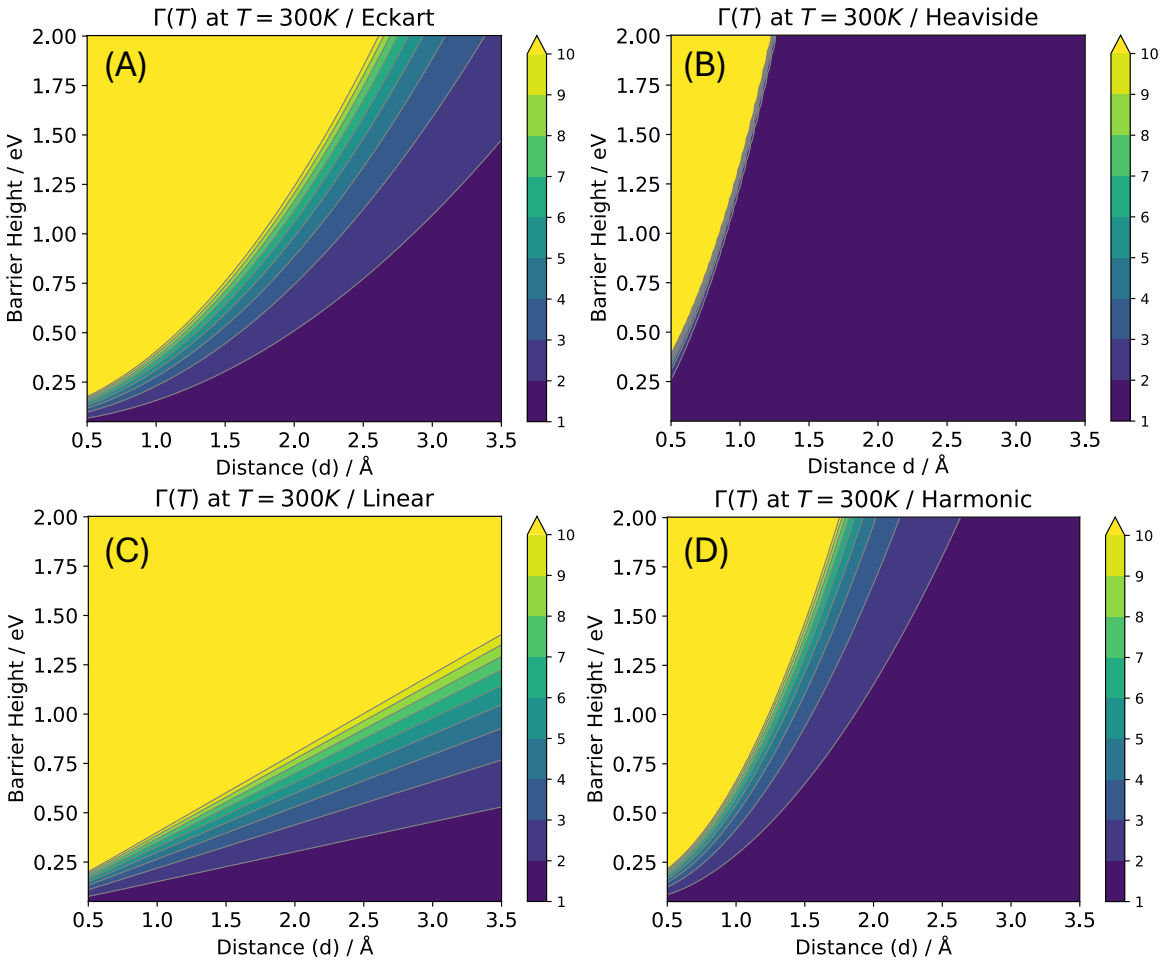

Figure 6: Tunneling correction factor $\Gamma(T)$ at T=300K given a symmetric barrier profile of (A) Eckart; (B) Heaviside; (C) Linear; (D) Harmonic.

Here we see that the specific form of the potential profile has a strong effect on the

behavior of Γ. Sharper energy surfaces, such as our 'linear' potential, admit significant tunneling rates even at relatively large distances, $d > 3$Å. In contrast, smoother potential profiles such as the harmonic and Eckart profiles will only exhibit tunneling for very short distances with moderate barrier heights, approximately $d < 2.0$Å. Finally, the widest profile, the Heaviside function, requires extremely short distances and very high barriers before tunneling overtakes the classical reaction rate. Details related to sensitivity analysis of the numerical integration can be found in SI Note 2.

As we illustrate in Figure 2, our calculated CPET MEPs are generally quite sharp, at times most comparable to the 'linear' profile. However, given uncertainty in determining an appropriate 'distance' metric for the CPET pathways, we model general behavior using the Eckart profile as it more closely matches the CPET MEP near the transition state, whereas the linear profile clearly deviates from the harmonic limit at the saddle point.

To probe the relevance of tunneling for CPET reactions at the electrified double layer, we computed MEPs for a variety of CPET reactions on several of transition metals, namely Pt, Cu, Ag, and Au. In particular, we calculated CPET reactions in alkaline and acidic media for (i) the Volmer reaction, i.e. $(H^+ + e^-) + * \rightarrow *H$ (ii) protonation of $*CO$ to form $*CHO$, and (iii) protonation of $*NO$ to form $*NOH$. In SI Note 3, we illustrate transition state geometries in chemical reactions using Figures S6 and S7.[79] Other reactions were also attempted, for example protonation of $*O$ to $*OH$ and $*N$ to $*NH$, but we were not able to localize a true saddle point under any of the tested conditions for these reactions. The chemistries probed here offer a balance of different proton acceptors and chemical relevance to sustainability. The Volmer reaction is highly important in green H_2 production, $*CO$ protonation for electroreduction of CO_2 (though our recent work suggests that formation of $*COH$ may be kinetically relevant as well), and $*NOH$ formation is thought to be rate determining for nitrate reduction to ammonia on some catalysts.[91] Figure 7 below illustrates the calculated barrier height and distances for the aforementioned reactions. We note that the reported barrier heights are at a potential such that the overall reaction is thermoneutral –

i.e., the reaction energy $\Delta G = 0$, as the reported Eckart potential is assumed to be symmetric here.

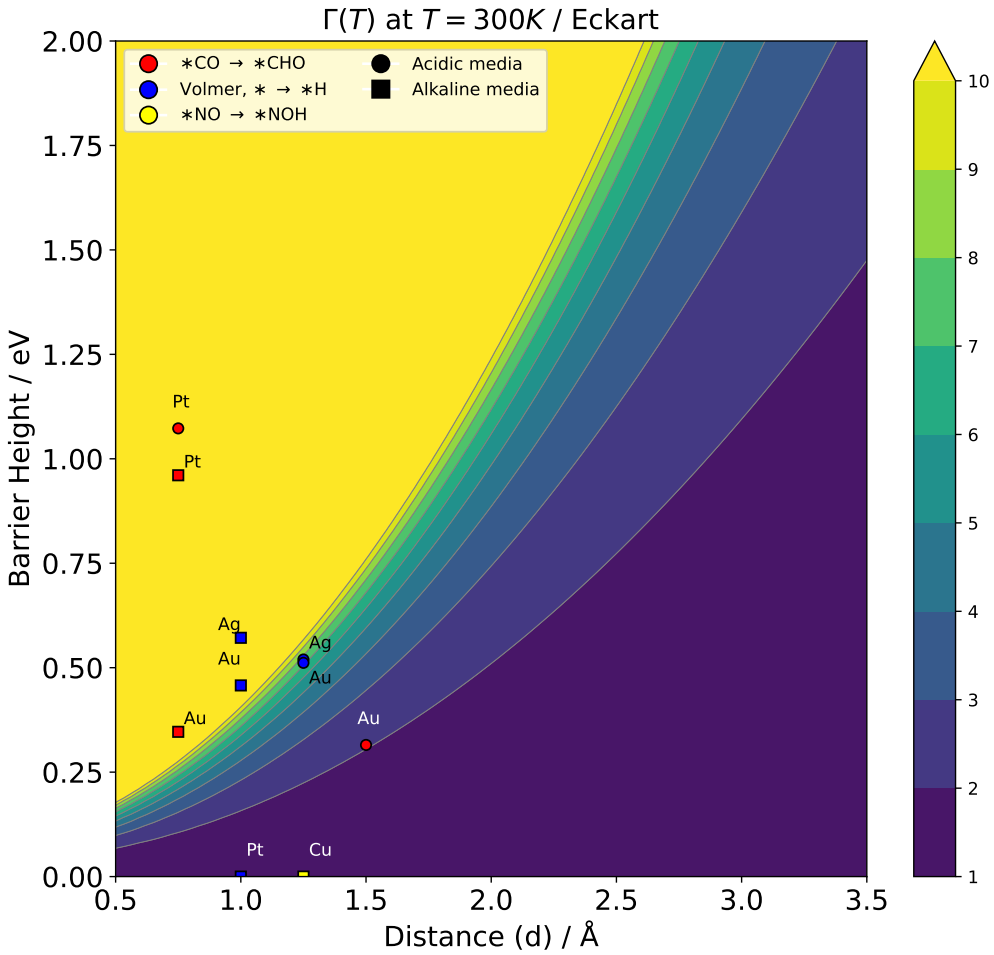

Figure 7: Role of tunneling for several CPET reactions at metal surfaces. Barrier heights shown are at an applied bias such that the overall reaction energy is zero, such that the symmetric Eckart potential is a reasonable approximation to the actual reaction coordinate. Here, yellow circles correspond to ∗NO→ ∗NOH, blue circles correspond to the Volmer reaction, and red circles correspond to ∗CO→ ∗CHO.

As we see in Figure 7, several well-studied CPET reactions fall in a region where our model predicts high rates of tunneling compared to the classical rate. In particular, reactions involving proton transfer to weak-binding metals (e.g., Volmer) and carbon, which show relatively high barriers and sufficiently short distances. Given previously published work on general trends in CPET activation barriers,[92] the above results suggest that CPET reactions

to carbon, nitrogen, and weak binding metals may experience significant tunneling rates. In contrast, proton transfer reactions to oxygen, which show very low barriers, are predicted to show minimal tunneling rates, in support of some experimental evidence,[93] as the classical rate is relatively fast.

Our model of proton tunneling is highly simplified in comparison to state-of-the-art methods for tunneling rates, typically utilized for molecular reactions.[2] For example, we neglect non-adiabatic effects (i.e., we invoke Born-Oppenheimer) such as contributions from reaction coordinate curvature and vibronic coupling. As such, we may be significantly underestimating the true tunneling contributions. Nevertheless, our simple model and approach for determining a characteristic tunneling distance reveals that several important reactions may be affected by high tunneling rates at ambient conditions.

As we discuss in more detail below, a particular reaction of interest in evaluating the role of proton tunneling is the HER on Au in alkaline media, as there is experimental evidence of substantial tunneling effects.[94] We therefore investigated the alkaline Volmer reaction more carefully, including the effect of applied overpotential on the calculated zero curvature tunneling correction factor, via consideration of the asymmetric Eckart potential, with the results illustrated in Figure 8.

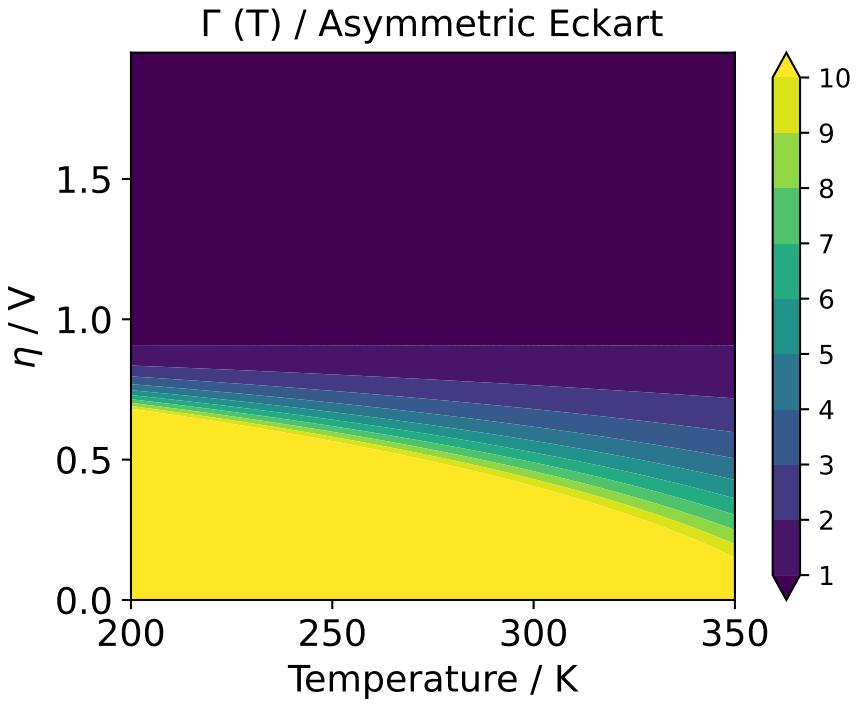

Figure 8: Role of tunneling for alkaline Volmer on Au (111). Here we predict significant tunneling contributions at near-ambient conditions and low overpotential

Our model predicts significant tunneling rates at near-ambient conditions and low overpotential, where the barrier is high. Given the very sharp MEP, under these conditions tunneling dominates the overall reaction rate – the classical rate is relatively slow. At high overpotential, the activation barrier reduces (with a slope of approximately 0.5 eV/V). As such, at high overpotential, our simple model predicts minimal tunneling, and the classical rate dominates the overall rate.

Kinetic isotopic effects for the hydrogen evolution reaction

Kinetic isotope effects (KIEs) for reactions involving hydrogen are typically measured experimentally as

$$\text{KIE} = \frac{r_H}{r_D} \quad , \tag{14}$$

where r_H refers to the reaction rate when using hydrogen, and r_D refers to the reaction rate upon replacing hydrogen with deuterium, which has twice the mass. KIEs can be caused by several factors, including significant quantum tunneling effects, making them observables of interest in validating our model. Classically, the reaction rate should be independent of the mass of a transferring hydrogen. However, the tunneling rate depends very strongly on the mass, as shown in Eq. 4. Experimental measurement of these effects are complicated by the fact that an observed reaction rate is a convolution of many elementary steps, even in the simplest of cases such as in the HER.[62,63] Observation of significant KIEs requires all rate-determining steps to experience significant quantum tunneling contributions. Additionally, non-electrochemical phenomena such as bubble formation and mass-transport limitations can complicate relating current density to fundamental quantities via, e.g., the Butler-Volmer equation.[63] As such, reported KIEs are mixed for even simple electrochemical processes[95] such as the HER.[93,94,96,97] To predict KIEs for the HER, we utilize our developed tunneling model to compute the ratio of zero curvature tunneling correction factors using hydrogen and deuterium as the tunneling species, i.e.,

$$\text{KIE} \approx \frac{\Gamma_H}{\Gamma_D} \quad , \tag{15}$$

where Γ_H is the zero curvature tunneling correction factor as defined in the previous sections, and Γ_D is the same quantity, but using deuterium instead of hydrogen. The results of our calculations, and experimental references[39,94,98,99] to compare against, are shown in Figure 9.

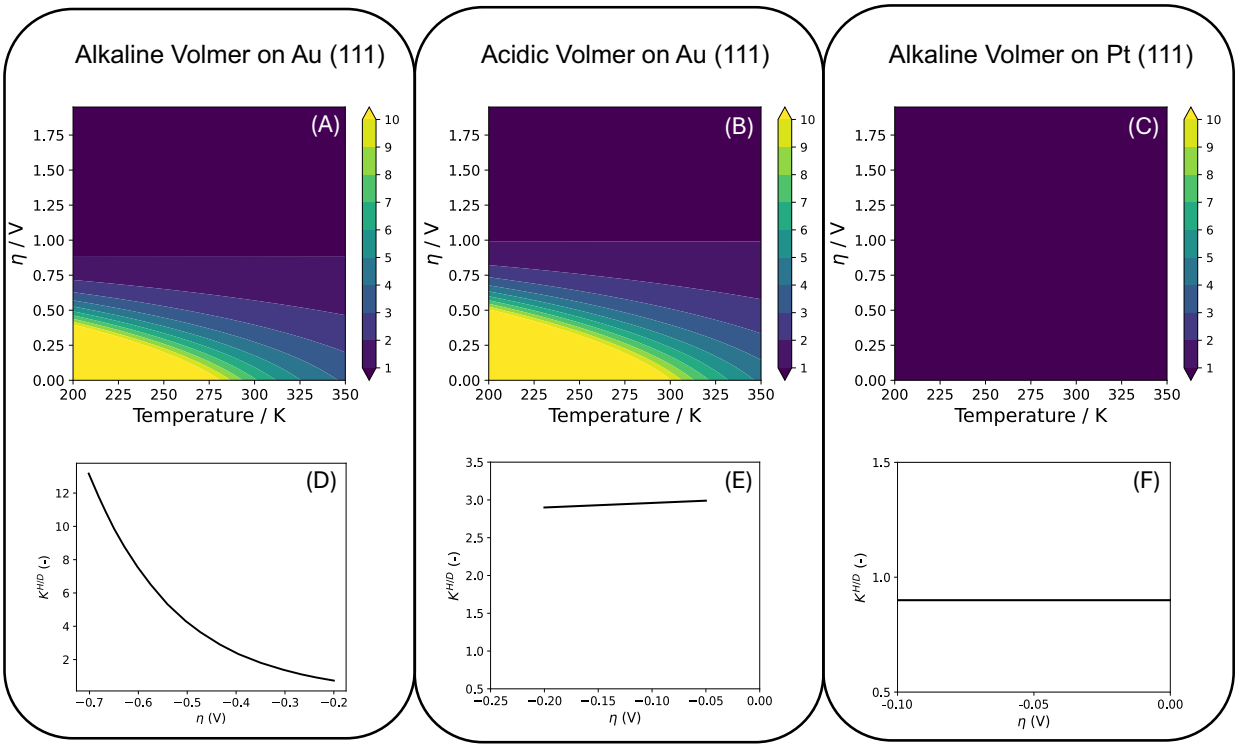

Figure 9: Comparison of Predicted Kinetic Isotopic Effect (KIE) for the Alkaline Volmer on Au (A), Acidic Volmer on Au (B), and Alkaline Volmer on Pt (C), with corresponding experimental data (panels D, E, and F respectively). Panels D, E, and F reproduced with permission from reference[94] with permission from the Royal Society of Chemistry. In the experimental reference, the symbol η represents the negative of our definition of η and are measured at $T = 298$ K.

In general, our model predicts low KIEs for most reactions at high overpotential, since the classical rate is uninhibited by the potential energy surface under these conditions. In practice, mass transport of reactants and products (particularly if they involve gaseous phases) may convolute measured KIEs under such conditions, explaining the limited potential windows in the experimental reference. In the case of acidic HER on Au (111) and alkaline HER on Pt (111), our model agrees reasonably well qualitatively and semi-quantitatively. The case of alkaline HER on Au (111) is different; here, significant tunneling effects are reported, and the magnitude of the KIE appears to exponentially increase with the applied overpotential. The data here was described as anomalous by the original authors,[94] and no additional datasets were found that corroborate this trend. Using a more sophisticated model of tunnel-

ing which incorporated non-adiabatic effects, Hammes-Schiffer[100] and coworkers found good agreement with this dataset, but with a lower slope, suggesting that non-adiabatic effects may dominate for this reaction.

Conclusions

To summarize, in this Article we presented a simple evaluation of the contribution of proton tunneling across the electrified double layer. Comparing calculated coupled proton-electron transfer reaction minimum energy paths to several archetypical barrier profiles, we find that none are an excellent match, as the calculated potential energy surface is extremely stiff – changing significantly over a very short length scale. However, approximating the MEP as an Eckart profile allows us to investigate general trends in zero curvature tunneling correction factors (Γ) as the barrier height and width change. Given the high sensitivity of the tunneling correction factor to the distance chosen, we presented a careful discussion on the appropriate choice of the distance. We argued that, for CPET reactions across the electrified double layer, taking the tunneling distance to be the O–H bond length for the transferring proton is a reasonable approximation. Based on our calculated CPET MEPs, this results in significantly shorter tunneling distances than those reported in early investigations. Our calculated tunneling correction factors suggest that for sufficiently high barriers – i.e., low overpotential regimes, particularly in alkaline media – CPETs may experience significant contributions from quantum tunneling effects. Given general trends observed in calculated CPET activation barriers, particularly that they appear to depend on the atom the proton is transferring to and from rather than the overall reaction energy,[92] we expect CPETs to weak-binding metal surfaces (e.g., Volmer), C, and N to experience significant tunneling at low overpotential. At high overpotential, our model suggests that tunneling declines as the barrier goes to zero and the classical rate increases. As such, CPETs involving proton transfer to oxygen (e.g., the oxygen reduction reaction) are found to have very low barri-

ers, and so tunneling is predicted to play a minimal role in these cases. We analyze the KIEs for the alkaline and acidic Volmer reactions on Au, and the alkaline reaction on Pt, comparing these calculations with experimental data.[94] While our model shows alignment with trends observed for the alkaline Volmer reaction on Pt and acidic Volmer on Au, our model is qualitatively incorrect for the alkaline Volmer reaction on Au. Overall, this analysis demonstrates the importance of non-adiabatic effects such as reaction coordinate curvature and vibronic coupling interactions for some reactions. The framework we developed makes several critical assumptions: we invoke the Born-Oppenheimer approximation, neglecting vibronic coupling contributions and reaction coordinate curvature. As a result, our calculated tunneling correction factors may be a significant underestimate of the true tunneling contributions. Nevertheless, our results provide a simple route to evaluate the role of proton tunneling for CPETs across the electrified double layer.

Supporting Information

All geometry files used in the DFT analysis, and all python codes used to produce figures found in the main text, can be found as a supporting zip archive. Additionally, a written SI document contains additional details related to the archetypical potential profiles investigated here, including a discussion of analytical forms of the classical turning points. We additionally present details related to sensitivity of numerical integration, demonstration of the reliability of the 1D-FBL method, and an illustration of the geometries of the transition states analyzed here.

Notes

The authors declare no competing financial interest.

Acknowledgments

The authors thank Professors Minh Nguyen, Vitaly Kiselev, and Shaama Sharada for helpful discussions related to the numerical treatment of the permeability function. This research used resources of the National Energy Research Scientific Computing Center (NERSC), a U.S. Department of Energy Office of Science User Facility located at Lawrence Berkeley National Laboratory, operated under Contract No. DE-AC02-05CH11231 using NERSC award BES-ERCAP0022848. The authors acknowledge the High Performance Computing Center (HPCC) at Texas Tech University for providing computational resources that have contributed to the research results reported within this paper. URL: http://www.hpcc.ttu.edu

References

(1) Warren, J. J.; Tronic, T. A.; Mayer, J. M. Thermochemistry of proton-coupled electron transfer reagents and its implications. *Chemical reviews* **2010**, *110*, 6961–7001.

(2) Warburton, R. E.; Soudackov, A. V.; Hammes-Schiffer, S. Theoretical modeling of electrochemical proton-coupled electron transfer. *Chemical Reviews* **2022**, *122*, 10599–10650.

(3) Li, J.; Stenlid, J. H.; Ludwig, T.; Lamoureux, P. S.; Abild-Pedersen, F. Modeling potential-dependent electrochemical activation barriers: revisiting the alkaline hydrogen evolution reaction. *Journal of the American Chemical Society* **2021**, *143*, 19341–19355.

(4) Masa, J.; Andronescu, C.; Schuhmann, W. Electrocatalysis as the nexus for sustainable renewable energy: the gordian knot of activity, stability, and selectivity. *Angewandte Chemie International Edition* **2020**, *59*, 15298–15312.

(5) Tang, C.; Zheng, Y.; Jaroniec, M.; Qiao, S.-Z. Electrocatalytic refinery for sustainable

production of fuels and chemicals. *Angewandte Chemie International Edition* **2021**, *60*, 19572–19590.

(6) Alerte, T.; Gaona, A.; Edwards, J. P.; Gabardo, C. M.; O'Brien, C. P.; Wicks, J.; Bonnenfant, L.; Rasouli, A. S.; Young, D.; Abed, J. et al. Scale-Dependent Techno-Economic Analysis of CO2 Capture and Electroreduction to Ethylene. *ACS Sustainable Chemistry & Engineering* **2023**, *11*, 15651–15662.

(7) De Luna, P.; Hahn, C.; Higgins, D.; Jaffer, S. A.; Jaramillo, T. F.; Sargent, E. H. What would it take for renewably powered electrosynthesis to displace petrochemical processes? *Science* **2019**, *364*, eaav3506.

(8) Deng, W.; Zhang, P.; Qiao, Y.; Kastlunger, G.; Govindarajan, N.; Xu, A.; Chorkendorff, I.; Seger, B.; Gong, J. Unraveling the rate-determining step of C2+ products during electrochemical CO reduction. *Nature Communications* **2024**, *15*, 892.

(9) Fisher, K. J.; Feuer, M. L.; Lant, H. M.; Mercado, B. Q.; Crabtree, R. H.; Brudvig, G. W. Concerted proton-electron transfer oxidation of phenols and hydrocarbons by a high-valent nickel complex. *Chemical Science* **2020**, *11*, 1683–1690.

(10) Nanni, L. Modelling proton tunneling in hydrogen bonds through path integral method. *Chemical Physics* **2023**, *574*, 112054.

(11) Kastlunger, G.; Lindgren, P.; Peterson, A. A. Controlled-potential simulation of elementary electrochemical reactions: Proton discharge on metal surfaces. *Journal of Physical Chemistry C* **2018**, *122*, 12771–12781.

(12) Skúlason, E.; Tripkovic, V.; Björketun, M. E.; Gudmundsdottir, S.; Karlberg, G.; Rossmeisl, J.; Bligaard, T.; Jónsson, H.; Nørskov, J. K. Modeling the electrochemical hydrogen oxidation and evolution reactions on the basis of density functional theory calculations. *The Journal of Physical Chemistry C* **2010**, *114*, 18182–18197.

(13) Akhade, S. A.; Bernstein, N. J.; Esopi, M. R.; Regula, M. J.; Janik, M. J. A simple method to approximate electrode potential-dependent activation energies using density functional theory. *Catalysis Today* **2017**, *288*, 63–73.

(14) Skúlason, E. Modeling electrochemical reactions at the solid-liquid interface using density functional calculations. *Procedia Computer Science* **2015**, *51*, 1887–1896.

(15) Chan, K.; Nørskov, J. K. Potential dependence of electrochemical barriers from ab initio calculations. *The Journal of Physical Chemistry Letters* **2016**, *7*, 1686–1690.

(16) Mathew, K.; Sundararaman, R.; Letchworth-Weaver, K.; Arias, T.; Hennig, R. G. Implicit solvation model for density-functional study of nanocrystal surfaces and reaction pathways. *The Journal of Chemical Physics* **2014**, *140*, 084106.

(17) Gauthier, J. A.; Dickens, C. F.; Chen, L. D.; Doyle, A. D.; Nørskov, J. K. Solvation effects for oxygen evolution reaction catalysis on IrO2 (110). *The Journal of Physical Chemistry C* **2017**, *121*, 11455–11463.

(18) Gauthier, J. A.; Ringe, S.; Dickens, C. F.; Garza, A. J.; Bell, A. T.; Head-Gordon, M.; Nørskov, J. K.; Chan, K. Challenges in Modeling Electrochemical Reaction Energetics with Polarizable Continuum Models. *ACS Catalysis* **2018**, *9*, 920–931.

(19) Gauthier, J. A.; Dickens, C. F.; Ringe, S.; Chan, K. Practical considerations for continuum models applied to surface electrochemistry. *ChemPhysChem* **2019**, *20*, 3074–3080.

(20) Gauthier, J. A.; Dickens, C. F.; Heenen, H. H.; Sudarshan, V.; Ringe, S.; Chan, K. Unified approach to implicit and explicit solvent simulations of electrochemical reaction energetics. *Journal of chemical theory and computation* **2019**,

(21) Gauthier, J. A.; Lin, Z.; Head-Gordon, M.; Bell, A. T. Pathways for the Formation

of C2+ Products under Alkaline Conditions during the Electrochemical Reduction of CO2. *ACS Energy Letters* **2022**, *7*, 1679–1686.

(22) Andreussi, O.; Dabo, I.; Marzari, N. Revised self-consistent continuum solvation in electronic-structure calculations. *The Journal of Chemical Physics* **2012**, *136*, 064102.

(23) Andreussi, O.; Marzari, N. Electrostatics of solvated systems in periodic boundary conditions. *Physical Review B* **2014**, *90*, 245101.

(24) Andreussi, O.; Hormann, N. G.; Nattino, F.; Fisicaro, G.; Goedecker, S.; Marzari, N. Solvent-aware interfaces in continuum solvation. *Journal of Chemical Theory and Computation* **2019**,

(25) Nocera, D. G. Proton-coupled electron transfer: the engine of energy conversion and storage. *Journal of the American Chemical Society* **2022**, *144*, 1069–1081.

(26) Darcy, J. W.; Kolmar, S. S.; Mayer, J. M. Transition state asymmetry in C–H bond cleavage by proton-coupled electron transfer. *Journal of the American Chemical Society* **2019**, *141*, 10777–10787.

(27) Usharani, D.; Lacy, D. C.; Borovik, A.; Shaik, S. Dichotomous hydrogen atom transfer vs proton-coupled electron transfer during activation of X–H bonds (X= C, N, O) by nonheme iron–oxo complexes of variable basicity. *Journal of the American Chemical Society* **2013**, *135*, 17090–17104.

(28) Mandal, M.; Elwell, C. E.; Bouchey, C. J.; Zerk, T. J.; Tolman, W. B.; Cramer, C. J. Mechanisms for hydrogen-atom abstraction by mononuclear copper (III) cores: Hydrogen-atom transfer or concerted proton-coupled electron transfer? *Journal of the American Chemical Society* **2019**, *141*, 17236–17244.

(29) Kastlunger, G.; Heenen, H. H.; Govindarajan, N. Combining First-Principles Kinetics

and Experimental Data to Establish Guidelines for Product Selectivity in Electrochemical CO2 Reduction. *ACS Catalysis* **2023**, *13*, 5062–5072.

(30) Kim, C.; Govindarajan, N.; Hemenway, S.; Park, J.; Zoraster, A.; Kong, C. J.; Prabhakar, R. R.; Varley, J. B.; Jung, H.-T.; Hahn, C. et al. Importance of Site Diversity and Connectivity in Electrochemical CO Reduction on Cu. *ACS Catalysis* **2023**, *14*, 3128–3138.

(31) Govindarajan, N.; Lin, T. Y.; Roy, T.; Hahn, C.; Varley, J. B. Coupling Microkinetics with Continuum Transport Models to Understand Electrochemical CO 2 Reduction in Flow Reactors. *PRX Energy* **2023**, *2*, 033010.

(32) Pasumarthi, V.; Yu, H.; Akhade, S. A.; Abild-Pedersen, F.; Varley, J. B.; Bajdich, M. A Comparative Study of Electrical Double Layer Effects for CO Reduction Reaction Kinetics. *The Journal of Physical Chemistry C* **2023**, *127*, 16850–16860.

(33) Lindgren, P.; Kastlunger, G.; Peterson, A. A. A Challenge to the G $\sim$ 0 Interpretation of Hydrogen Evolution. *ACS Catalysis* **2020**, *10*, 121–128.

(34) Chen, X.; El Khatib, M.; Lindgren, P.; Willard, A.; Medford, A. J.; Peterson, A. A. Atomistic learning in the electronically grand-canonical ensemble. *npj Computational Materials* **2023**, *9*, 73.

(35) Collinge, G.; Yuk, S. F.; Nguyen, M.-T.; Lee, M.-S.; Glezakou, V.-A.; Rousseau, R. Effect of collective dynamics and anharmonicity on entropy in heterogenous catalysis: Building the case for advanced molecular simulations. *ACS Catalysis* **2020**, *10*, 9236–9260.

(36) Bramley, G. A.; Nguyen, M.-T.; Glezakou, V.-A.; Rousseau, R.; Skylaris, C.-K. Understanding adsorption of organics on pt (111) in the aqueous phase: insights from dft based implicit solvent and statistical thermodynamics models. *Journal of Chemical Theory and Computation* **2022**, *18*, 1849–1861.

(37) Georgievskii, Y.; Klippenstein, S. J. Entanglement Effect and Angular Momentum Conservation in a Nonseparable Tunneling Treatment. *Journal of Chemical Theory and Computation* **2021**, *17*, 3863–3885.

(38) Steinfeld, J. I.; Francisco, J. S.; Hase, W. L. *Chemical Kinetics and dynamics*; Prentice Hall, 1998.

(39) Kiefer, P. M.; Hynes, J. T. Kinetic isotope effects for nonadiabatic proton transfer reactions in a polar environment. 1. Interpretation of tunneling kinetic isotopic effects. *The Journal of Physical Chemistry A* **2004**, *108*, 11793–11808.

(40) Che, L.; Ren, Z.; Wang, X.; Dong, W.; Dai, D.; Wang, X.; Zhang, D. H.; Yang, X.; Sheng, L.; Li, G. et al. Breakdown of the Born-Oppenheimer Approximation in the F+ o-D2→ DF+ D Reaction. *Science* **2007**, *317*, 1061–1064.

(41) Alexander, M. H.; Capecchi, G.; Werner, H.-J. Theoretical study of the validity of the Born-Oppenheimer approximation in the Cl+ H2→ HCl+ H reaction. *Science* **2002**, *296*, 715–718.

(42) Zheng, R.; Jing, Y.; Chen, L.; Shi, Q. Theory of proton coupled electron transfer reactions: Assessing the Born–Oppenheimer approximation for the proton motion using an analytically solvable model. *Chemical Physics* **2011**, *379*, 39–45.

(43) Kiefer, P. M.; Hynes, J. T. Kinetic isotope effects for adiabatic proton transfer reactions in a polar environment. *The Journal of Physical Chemistry A* **2003**, *107*, 9022–9039.

(44) Koper, M.; Mohr, J.-H.; Schmickler, W. Quantum effects in adiabatic electrochemical electron-transfer reactions. *Chemical physics* **1997**, *220*, 95–114.

(45) Logadóttir, Á.; Nørskov, J. K. Ammonia synthesis over a Ru (0001) surface studied by density functional calculations. *Journal of Catalysis* **2003**, *220*, 273–279.

(46) van Harrevelt, R.; Honkala, K.; Nørskov, J. K.; Manthe, U. The reaction rate for dissociative adsorption of N2 on stepped Ru (0001): six-dimensional quantum calculations. *The Journal of chemical physics* **2005**, *122*.

(47) Romm, L.; Katz, G.; Kosloff, R.; Asscher, M. Dissociative chemisorption of N2 on Ru (001) enhanced by vibrational and kinetic energy: Molecular beam experiments and quantum mechanical calculations. *The Journal of Physical Chemistry B* **1997**, *101*, 2213–2217.

(48) Waluk, J. Nuclear Quantum Effects in Proton or Hydrogen Transfer. *The Journal of Physical Chemistry Letters* **2024**, *15*, 598–607.

(49) Topley, B.; Eyring, H. Electrolytic Separation of Hydrogen Isotopes and the Mechanism of the Cathode Process. *Journal of the American Chemical Society* **1933**, *55*, 5058–5059.

(50) Bawn, C.; Ogden, G. Wave mechanical effects and the reactivity of the hydrogen isotopes. *Transactions of the Faraday Society* **1934**, *30*, 432–443.

(51) St G, C. Einige fragen der tunneltheorie der Wasserstoffüberspannung—I. Die gültigkeitsbedin-gungen der tafelschen gleichung und die grösse der quanteneffekte. *Electrochimica Acta* **1961**, *4*, 194–214.

(52) Conway, B. Some considerations on the role of proton tunneling in certain charge transfer processes. *Canadian Journal of Chemistry* **1959**, *37*, 178–189.

(53) Bockris, J. O.; Matthews, D. B. Proton Tunneling in the Hydrogen-Evolution Reaction. *The Journal of Chemical Physics* **1966**, *44*, 298–309.

(54) Eckart, C. The penetration of a potential barrier by electrons. *Physical Review* **1930**, *35*, 1303.

(55) Misicu, S. Quantum tunneling with dissipation in smoothly joined parabolic potential. *arXiv preprint quant-ph/9906012* **1999**,

(56) Misicu, S. Quantum tunneling with dissipation in quadratic potentials. **1999**,

(57) Isar, A. Dissipative Tunnelling Through a Parabolic Potential in the Theory of Open Quantum Systems. **2000**,

(58) López, Á. G.; Valani, R. N. Unpredictable tunneling in a retarded bistable potential. *Chaos: An Interdisciplinary Journal of Nonlinear Science* **2024**, *34*.

(59) Garashchuk, S.; Gu, B.; Mazzuca, J. Calculation of the quantum-mechanical tunneling in bound potentials. *Journal of Theoretical Chemistry* **2014**, *2014*.

(60) Liu, D.-Q.; Kang, M.; Perry, D.; Chen, C.-H.; West, G.; Xia, X.; Chaudhuri, S.; Laker, Z. P.; Wilson, N. R.; Meloni, G. N. et al. Adiabatic versus non-adiabatic electron transfer at 2D electrode materials. *Nature Communications* **2021**, *12*, 7110.

(61) Liu, T.; Guo, M.; Orthaber, A.; Lomoth, R.; Lundberg, M.; Ott, S.; Hammarström, L. Accelerating proton-coupled electron transfer of metal hydrides in catalyst model reactions. *Nature Chemistry* **2018**, *10*, 881–887.

(62) Zeradjanin, A. R.; Grote, J.-P.; Polymeros, G.; Mayrhofer, K. J. A critical review on hydrogen evolution electrocatalysis: Re-exploring the volcano-relationship. *Electroanalysis* **2016**, *28*, 2256–2269.

(63) Zeradjanin, A. R.; Narangoda, P.; Masa, J.; Schlögl, R. What Controls Activity Trends of Electrocatalytic Hydrogen Evolution Reaction?- Activation Energy Versus Frequency Factor. *ACS Catalysis* **2022**, *12*, 11597–11605.

(64) Wu, T.; Sun, M.; Wong, H. H.; Chan, C. H.; Lu, L.; Lu, Q.; Chen, B.; Huang, B. Recent Advances and Strategies of Electrocatalysts for Large Current Density Industrial Hydrogen Evolution Reaction. *Inorganic Chemistry Frontiers* **2023**,

(65) Hu, W.-P.; Liu, Y.-P.; Truhlar, D. G. Variational transition-state theory and semiclassical tunnelling calculations with interpolated corrections: A new approach to interfacing electronic structure theory and dynamics for organic reactions. *Journal of the Chemical Society, Faraday Transactions* **1994**, *90*, 1715–1725.

(66) Biswas, D.; Ramachandran, R. Curvature correction to the field emission current. *Journal of Vacuum Science & Technology B* **2019**, *37*.

(67) Kresse, G.; Hafner, J. Ab initio molecular dynamics for liquid metals. *Physical Review B* **1993**, *47*, 558.

(68) Kresse, G.; Furthmüller, J. Efficiency of ab-initio total energy calculations for metals and semiconductors using a plane-wave basis set. *Computational Materials Science* **1996**, *6*, 15–50.

(69) Kresse, G.; Furthmüller, J. Efficient iterative schemes for ab initio total-energy calculations using a plane-wave basis set. *Physical Review B* **1996**, *54*, 11169.

(70) Larsen, A. H.; Mortensen, J. J.; Blomqvist, J.; Castelli, I. E.; Christensen, R.; Dułak, M.; Friis, J.; Groves, M. N.; Hammer, B.; Hargus, C. The atomic simulation environment—a Python library for working with atoms. *Journal of Physics: Condensed Matter* **2017**, *29*, 273002.

(71) Kresse, G.; Joubert, D. From ultrasoft pseudopotentials to the projector augmented-wave method. *Physical Review B* **1999**, *59*, 1758.

(72) Larsen, A. H.; Mortensen, J. J.; Blomqvist, J.; Castelli, I. E.; Christensen, R.; Dułak, M.; Friis, J.; Groves, M. N.; Hammer, B.; Hargus, C. et al. The atomic simulation environment—a Python library for working with atoms. *Journal of Physics: Condensed Matter* **2017**, *29*, 273002.

(73) Hammer, B.; Hansen, L. B.; Nørskov, J. K. Improved adsorption energetics within density-functional theory using revised Perdew-Burke-Ernzerhof functionals. *Physical Review B* **1999**, *59*, 7413.

(74) Monkhorst, H. J.; Pack, J. D. Special points for Brillouin-zone integrations. *Physical Review B* **1976**, *13*, 5188.

(75) Gauthier, J. A.; Chen, L. D.; Bajdich, M.; Chan, K. Implications of the fractional charge of hydroxide at the electrochemical interface. *Physical Chemistry Chemical Physics* **2020**, *22*, 6964–6969.

(76) Mathew, K.; Kolluru, V. C.; Mula, S.; Steinmann, S. N.; Hennig, R. G. Implicit self-consistent electrolyte model in plane-wave density-functional theory. *The Journal of Chemical Physics* **2019**, *151*, 234101.

(77) Steinmann, S. N.; Seh, Z. W. Understanding electrified interfaces. *Nature Reviews Materials* **2021**, *6*, 289–291.

(78) Ringe, S.; Hormann, N. G.; Oberhofer, H.; Reuter, K. Implicit solvation methods for catalysis at electrified interfaces. *Chemical Reviews* **2021**, *122*, 10777–10820.

(79) Henkelman, G.; Uberuaga, B. P.; Jónsson, H. A climbing image nudged elastic band method for finding saddle points and minimum energy paths. *The Journal of Chemical Physics* **2000**, *113*, 9901–9904.

(80) Gauthier, J. A. Common functions useful in Gauthier lab. 2021; `https://github.com/gauthierlab/common/`.

(81) Henkelman, G.; Jónsson, H. A dimer method for finding saddle points on high dimensional potential surfaces using only first derivatives. *The Journal of chemical physics* **1999**, *111*, 7010–7022.

(82) Trasatti, S. The absolute electrode potential: an explanatory note (Recommendations 1986). *Pure and Applied Chemistry* **1986**, *58*, 955–966.

(83) Goodpaster, J. D.; Bell, A. T.; Head-Gordon, M. Identification of possible pathways for C–C bond formation during electrochemical reduction of CO2: New theoretical insights from an improved electrochemical model. *The Journal of Physical Chemistry Letters* **2016**, *7*, 1471–1477.

(84) Jinnouchi, R.; Anderson, A. B. Aqueous and surface redox potentials from self-consistently determined Gibbs energies. *The Journal of Physical Chemistry C* **2008**, *112*, 8747–8750.

(85) Duan, Z.; Xiao, P. Simulation of Potential-Dependent Activation Energies in Electrocatalysis: Mechanism of O–O Bond Formation on RuO2. *The Journal of Physical Chemistry C* **2021**, *125*, 15243–15250.

(86) Fernandez-Ramos, A.; Ellingson, B. A.; Garrett, B. C.; Truhlar, D. G. Variational transition state theory with multidimensional tunneling. *Reviews in computational chemistry* **2007**, *23*, 125.

(87) Bac, S.; Quiton, S. J.; Kron, K. J.; Chae, J.; Mitra, U.; Mallikarjun Sharada, S. A matrix completion algorithm for efficient calculation of quantum and variational effects in chemical reactions. *The Journal of Chemical Physics* **2022**, *156*.

(88) Santos, E.; Aradi, B.; van der Heide, T.; Schmickler, W. Free energy curves for the Volmer reaction obtained from molecular dynamics simulation based on quantum chemistry. *Journal of Electroanalytical Chemistry* **2024**, *954*, 118044.

(89) Chen, L. D.; Bajdich, M.; Martirez, J. M. P.; Krauter, C. M.; Gauthier, J. A.; Carter, E. A.; Luntz, A. C.; Chan, K.; Nørskov, J. K. Understanding the apparent fractional charge of protons in the aqueous electrochemical double layer. *Nature Communications* **2018**, *9*, 3202.

(90) Hait, D.; Head-Gordon, M. When Is a Bond Broken? The Polarizability Perspective. *Angewandte Chemie International Edition* **2023**, *62*, e202312078.

(91) Kani, N. C.; Gauthier, J. A.; Prajapati, A.; Edgington, J.; Bordawekar, I.; Shields, W.; Shields, M.; Seitz, L. C.; Singh, A. R.; Singh, M. R. Solar-driven electrochemical synthesis of ammonia using nitrate with 11% solar-to-fuel efficiency at ambient conditions. *Energy & Environmental Science* **2021**, *14*, 6349–6359.

(92) Patel, A. M.; Vijay, S.; Kastlunger, G.; Nørskov, J. K.; Chan, K. Generalizable trends in electrochemical protonation barriers. *The Journal of Physical Chemistry Letters* **2021**, *12*, 5193–5200.

(93) Rebollar, L.; Intikhab, S.; Snyder, J. D.; Tang, M. H. Kinetic isotope effects quantify pH-sensitive water dynamics at the Pt electrode interface. *The Journal of Physical Chemistry Letters* **2020**, *11*, 2308–2313.

(94) Sakaushi, K. Quantum proton tunneling in multi-electron/-proton transfer electrode processes. *Faraday Discussions* **2020**, *221*, 428–448.

(95) He, Z.-D.; Chen, Y.-X.; Santos, E.; Schmickler, W. The Pre-exponential Factor in Electrochemistry. *Angewandte Chemie International Edition* **2018**, *57*, 7948–7956.

(96) Andersson, S.; Goumans, T.; Arnaldsson, A. Tunneling in hydrogen and deuterium atom addition to CO at low temperatures. *Chemical Physics Letters* **2011**, *513*, 31–36.

(97) Zhang, W.; Burgess, I. J. Kinetic isotope effects in proton coupled electron transfer. *Journal of Electroanalytical Chemistry* **2012**, *668*, 66–72.

(98) Yang, Y.; Peltier, C. R.; Zeng, R.; Schimmenti, R.; Li, Q.; Huang, X.; Yan, Z.; Potsi, G.; Selhorst, R.; Lu, X. et al. Electrocatalysis in alkaline media and alkaline membrane-based energy technologies. *Chemical Reviews* **2022**, *122*, 6117–6321.

(99) Kumeda, T.; Sakaushi, K. Cation-Dependent Nonadiabaticity in Proton-Coupled Electron Transfer at Electrified Solid-Liquid Interfaces. *arXiv preprint arXiv:2207.00138* **2022**,

(100) Lam, Y.-C.; Soudackov, A. V.; Hammes-Schiffer, S. Theory of electrochemical proton-coupled electron transfer in diabatic vibronic representation: application to proton discharge on metal electrodes in alkaline solution. *The Journal of Physical Chemistry C* **2020**, *124*, 27309–27322.

Graphical TOC Entry